Inorganic Chemistry

Article

pubs.acs.org/IC

Mn^{II} Coordination Polymers Based on Bi-, Tri-, and Tetranuclear and Polymeric Chain Building Units: Crystal Structures and Magnetic Properties

Lu-Fang Ma,[†] Min-Le Han,[†] Jian-Hua Qin,[†] Li-Ya Wang,*[,†,‡] and Miao Du*[,§]

[†]College of Chemistry and Chemical Engineering, Luoyang Normal University, Luoyang 471022, P. R. China

[‡]College of Chemistry and Pharmaceutical Engineering, Nanyang Normal University, Nanyang 473061, P. R. China

[§]College of Chemistry, Tianjin Key Laboratory of Structure and Performance for Functional Molecule, Tianjin Normal University, Tianjin 300387, P. R. China

Supporting Information

ABSTRACT: Five new Mn^{II} coordination polymers, namely $[Mn_2(tbip)_2(bix)]$ (**1**), $[Mn_3(tbip)_3(bix)_2]$ (**2**), $[Mn_3(tbip)_2(Htbip)_2(bib)_2]\cdot 4H_2O$ (**3**), $[Mn_4(tbip)_4(bbp)_2(H_2O)_2]$ (**4**), and $[Mn_4(tbip)_4(bip)]\cdot 2H_2O$ (**5**), were prepared by hydrothermal reactions of Mn(II) acetate with H_2tbip (5-*tert*-butyl isophthalic acid) in the presence of different di-imidazolyl coligands (bix = 1,4-bis(imidazol-1-ylmethyl)benzene, bib =1,4-bis(imidazol) butane, bbp =1,3-bis(benzimidazol)propane, bip =1,3-bis-(imidazol)propane). All complexes were characterized by elemental analysis, IR spectra, thermogravimetric analysis, single-crystal X-ray crystallography, and powder X-ray diffraction. Single crystal X-ray studies show that these coordination polymers contain homometallic clusters varying from dimeric, trimeric, and tetrameric motifs to polymeric chains depending upon the coligands used. Complex **1** has a 3D 6-connected polycatenane network with dinuclear $[Mn_2O_2]$ secondary building units. Complex **2** possesses a 3D 8-connected structure with trinuclear $[Mn_3(COO)_6]$ units. Complex **3** shows a 3D **pcu** net based on trinuclear $[Mn_3(COO)_6]$ clusters as nodes. Complex **4** features a 3D 8-connected structure constructed from the distorted square-grid tetranuclear $[Mn_4(\mu_2\text{-}COO)_8(\mu_2\text{-}H_2O)]$ units. Complex **5** shows a 3D (4,5,6)-connected net containing 1D μ-O/μ-COO alternately bridged chains. Magnetic susceptibility measurements indicate that complexes **1** and **3**−**5** show weak antiferromagnetic interactions between the adjacent Mn^{II} ions, whereas **2** is a three-spin center homometallic ferromagnetic system.

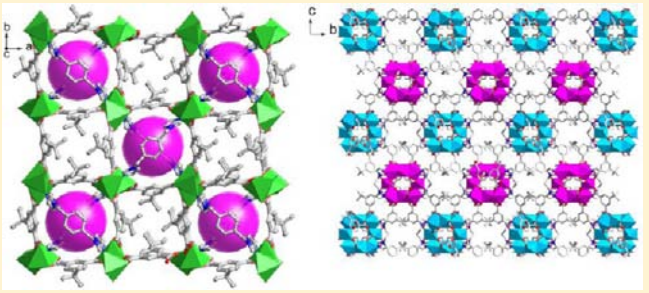

INTRODUCTION

Recently, a certain amount of attention has been paid to the use of multimetallic clusters as building units in synthesis of metal−organic hybrid materials because they have provided substantial impetus for development in a wide range of fields.[1−5] In practice, most of these materials are achieved by linking the transition metal ions through multidentate bridging ligands.[6,7] The nature of the organic bridging ligand is crucial to govern the nuclearity and arrangement of metal complexes. For example, isophthalate and its derivatives with specific conformations and versatile coordination fashions can bind several metal centers of specific coordination geometry to construct polynuclear clusters.[8] Zhou et al.[9] prepared a graphitic MOF structure (MAMS) containing octanickel $[Ni_8(\mu_3\text{-}OH)_4]$ clusters by reacting 5-*tert*-butyl isophthalic acid with $Ni(NO_3)_2$ in a solvothermal reaction, which can separate any two or more gases with kinetic diameters between 2.9 and 5.0 Å through temperature-controlled molecular gating to hydrophobic gas-storage chambers. Du et al.[10] reported a new ferromagnetic Mn^{II}-carboxylate coordination polymer with 5-tert-butyl isophthalic acid constructed from trinuclear Mn^{II} subunits. This compound is a three-spin center homometallic ferromagnetic complex with a (5/2, 10/2) spin topology and a $^1/_3$ magnetization plateau.

Meanwhile, carboxylato-bridged Mn^{II} complexes are of special interests, since such systems are known to exist at the active centers of some Mn^{II}-containing enzymes.[11] Moreover, these Mn^{II} complexes are well recognized from the magnetic point of view as the high-spin Mn^{II} contains up to five unpaired electrons, and thus the assembly of Mn^{II} with multicarboxylate is inclined to the formation of larger clusters and extended solids, such as Mn_2, Mn_3, Mn_4, Mn_6, Mn_{12}, and Mn−O−C−O−Mn chain.[12,13] However, the rational synthesis of such complexes is still a great challenge. Recently, we have successfully prepared a series of Mn^{II} coordination polymers derived from isophthalate derivatives and dipyridyl coligands, which contain bi- or trinuclear clusters.[14]

In order to extend our investigations in this field, herein we report the syntheses, crystal structures, and magnetic properties of five new polymeric coordination frameworks,

Received: June 12, 2012
Published: August 21, 2012

   dx.doi.org/10.1021/ic3012537 | *Inorg. Chem.* 2012, 51, 9431−9442

Scheme 1. Synthesis of Complexes 1−5 (I: $Mn^{II}/H_2tbip/bix$ = 1/1/1; II: $Mn^{II}/H_2tbip/bix$ = 2/1/1, AF = Antiferromagnetic Interaction, F = Ferromagnetic Interaction)

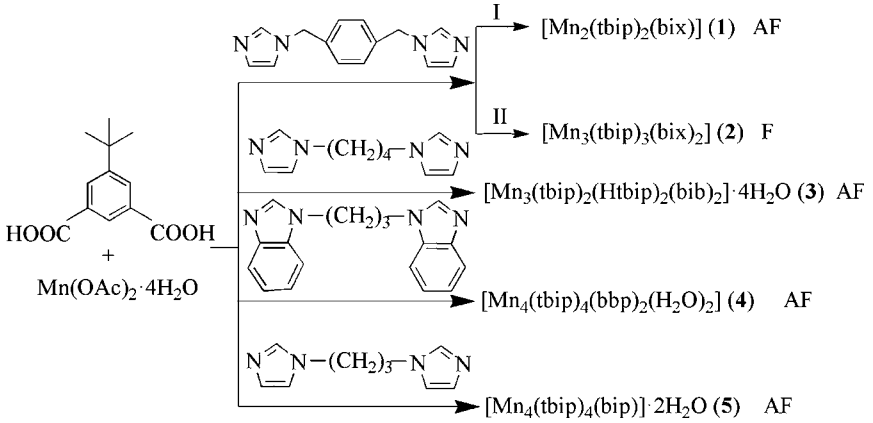

Table 1. Crystallographic Data and Structure Refinement Details for 1−5

	1	2	3	4	5
formula	$C_{38}H_{38}Mn_2N_4O_8$	$C_{64}H_{64}Mn_3N_8O_{12}$	$C_{68}H_{86}Mn_3N_8O_{20}$	$C_{82}H_{82}Mn_4N_8O_{17}$	$C_{57}H_{64}Mn_4N_4O_{18}$
fw	788.60	1302.05	1500.26	1671.32	1312.88
T	296(2)	296(2)	296(2)	296(2)	296(2)
cryst syst	tetragonal	orthorhombic	triclinic	monoclinic	orthorhombic
space group	$P4_2/n$	$Ama2$	$P\bar{1}$	$C2/c$	$Fddd$
a (Å)	20.0641(8)	33.611(3)	9.6461(14)	19.493(6)	11.6083(8)
b (Å)	20.0641(8)	13.8679(14)	14.257(2)	29.829(9)	40.268(3)
c (Å)	8.8106(7)	13.7856(14)	14.544(2)	16.340(5)	48.394(3)
α (deg)	90	90	109.208(2)	90	90
β (deg)	90	90	105.505(2)	125.281(3)	90
γ (deg)	90	90	92.453(2)	90	90
V (Å^3)	3546.9(3)	6425.7(11)	1801.3(5)	7756(4)	22621(3)
Z	4	4	2	8	16
D_c (g cm^{-3})	1.477	1.346	1.383	1.431	1.542
μ (mm^{-1})	0.771	0.646	0.594	0.711	0.951
F (000)	1632	2700	785	3464	10 848
θ range/deg	2.52−25.50	2.41−25.50	2.50−25.50	2.42−25.50	2.36−25.50
reflns collected	25 649	22 436	13 609	22 141	32 789
indep reflns	3309	6086	6631	7136	5267
R_{int}	0.0348	0.0499	0.0291	0.0562	0.0299
data/restraints/params	3309/0/238	6086/118/417	6631/18/455	7136/69/524	5267/78/408
GOF	1.017	1.011	1.022	1.042	1.028
R1,[a] wR2[b] [$I > 2\sigma(I)$]	0.0299, 0.0749	0.0395, 0.0868	0.0504, 0.1317	0.0753, 0.2101	0.0435, 0.1584
R1, wR2 (all data)	0.0395, 0.0811	0.0534, 0.0938	0.0708, 0.1458	0.0990, 0.2293	0.0512, 0.1745
$\Delta\rho_{max}$ and $\Delta\rho_{min}$ (e Å^{-3})	0.224, −0.233	0.304, −0.332	0.895, −0.703	1.564, −0.853	0.976, −0.725

[a] $R1 = \Sigma(|F_o| - |F_c|)/\Sigma|F_o|$. [b] $wR2 = \{\Sigma[w(|F_o|^2 - |F_c|^2)^2]/\Sigma[w(|F_o|^2)^2]\}^{1/2}$.

$[Mn_2(tbip)_2(bix)]$ (**1**), $[Mn_3(tbip)_3(bix)_2]$ (**2**), $[Mn_3(tbip)_2(Htbip)_2(bib)_2]\cdot 4H_2O$ (**3**), $[Mn_4(tbip)_4(bbp)_2(H_2O)_2]$ (**4**), and $[Mn_4(tbip)_4(bip)]\cdot 2H_2O$ (**5**) (see Scheme 1). All these complexes were characterized by X-ray crystallographic, IR, elemental, thermal stability, and powder X-ray diffraction analyses. The magnetic properties of **1**−**5** were also investigated and discussed in detail.

EXPERIMENTAL SECTION

Materials and Physical Measurements. All reagents were commercially available and used as received. All the products are stable in air at ambient conditions. Elemental analyses for C, H, and N were performed on a Flash 2000 organic elemental analyzer. Thermogravimetric analysis was performed on a SII EXStar6000 TG/DTA6300 analyzer heated from 30 to 900 °C under a dry nitrogen atmosphere with a heating rate of 10 °C min^{-1}. The infrared spectra (4000−600 cm^{-1}) were recorded on a NICOLET 6700 FT-IR spectrometer. Powder X-ray diffraction (PXRD) patterns were taken on a Bruker D8-ADVANCE X-ray diffractometer with Cu Kα radiation (λ = 1.5418 Å). Variable-temperature magnetic measurements were performed on a Quantum Design SQUID MPMS XL-7 instrument in a magnetic field of 2000 Oe in the temperature of 2−300 K. Diamagnetic corrections were made with Pascal's constants for all constituent atoms.

Preparation of Complexes 1−5. $[Mn_2(tbip)_2(bix)]$ (1). A mixture of H_2tbip (0.1 mmol, 23.1 mg), bix (0.1 mmol, 23.8 mg), $Mn(OAc)_2\cdot 4H_2O$ (0.1 mmol, 24.2 mg), KOH (0.1 mmol, 5.6 mg), and H_2O (12 mL) was placed in a Teflon-lined stainless steel vessel, heated to 140 °C for 3 days, and then cooled to room temperature over 24 h. Colorless block crystals of **1** were obtained. Yield: 19.7 mg, 50% (based on Mn^{II}). Anal. (%) Calcd for $C_{38}H_{38}Mn_2N_4O_8$: C 57.88, H 4.86, N 7.10. Found: C 57.94, H 4.81, N 7.15. IR (cm^{-1}): 3139 m, 2962 m, 1608 m, 1560 m, 1536 s, 1455 m, 1427 m, 1358 s, 1087 s, 777 s, 736 s, 709 m, 660 s.

dx.doi.org/10.1021/ic3012537 | Inorg. Chem. 2012, 51, 9431−9442

Table 2. Selected Bond Lengths (Å) and Angles (deg) for 1−5[a]

1			
Mn1−O1	2.1278(15)	Mn1−O3#2	2.2041(13)
Mn1−N1	2.1584(16)	Mn1−O3#1	2.1590(13)
Mn1−O2	2.3392(15)	Mn1−O4#2	2.3444(14)
O1−Mn1−N1	92.09(6)	O1−Mn1−O3#1	120.53(6)
N1−Mn1−O3#1	90.36(6)	O1−Mn1−O3#2	157.52(5)
N1−Mn1−O3#2	102.76(6)	O3#1−Mn1−O3#2	76.69(5)
O1−Mn1−O2	58.22(5)	N1−Mn1−O2	149.18(6)
O3#1−Mn1−O2	97.75(6)	O3#2−Mn1−O2	108.03(5)
O1−Mn1−O4#2	102.50(6)	N1−Mn1−O4#2	109.00(6)
O3#1−Mn1−O4#2	132.21(5)	O3#2−Mn1−O4#2	56.87(5)
O2−Mn1−O4#2	87.29(6)		
2			
Mn1−O1	2.144(3)	Mn1−N3#1	2.197(3)
Mn1−N1	2.211(3)	Mn1−O5	2.223(3)
Mn1−O4#2	2.287(2)	Mn1−O6	2.306(2)
Mn2−O4#3	2.212(2)	Mn2−O4#2	2.212(2)
Mn2−O2#4	2.217(3)	Mn2−O2	2.217(3)
O1−Mn1−N3#1	92.47(12)	O1−Mn1−N1	114.75(11)
N3#1−Mn1−N1	147.05(12)	O1−Mn1−O5	89.13(11)
N3#1−Mn1−O5	111.26(12)	N1−Mn1−O5	88.45(12)
O1−Mn1−O4#2	75.66(9)	N3#1−Mn1−O4#2	85.72(11)
N1−Mn1−O4#2	83.66(10)	O5−Mn1−O4#2	157.90(10)
O1−Mn1−O6	141.17(10)	N3#1−Mn1−O6	82.67(11)
N1−Mn1−O6	86.52(11)	O5−Mn1−O6	57.88(11)
O4#2−Mn1−O6	141.55(10)	O4#3−Mn2−O4#2	123.61(13)
O4#3−Mn2−O2#4	122.95(9)	O4#2−Mn2−O2#4	95.05(10)
O4#3−Mn2−O2	95.05(10)	O4#2−Mn2−O2	122.95(9)
O2#4−Mn2−O2	96.04(16)		
3			
Mn1−O7#1	2.098(2)	Mn2−O1	2.119(2)
Mn1−O7#2	2.098(2)	Mn2−O8#2	2.176(2)
Mn1−O2#3	2.143(2)	Mn2−N3	2.223(3)
Mn1−O2	2.143(2)	Mn2−N1	2.257(3)
Mn1−O5#3	2.249(2)	Mn2−O5	2.301(2)
Mn1−O5	2.249(2)	Mn2−O6	2.334(2)
O7#1−Mn1−O7#2	180	O1−Mn2−O8#2	97.56(10)
O7#1−Mn1−O2#3	93.64(10)	O1−Mn2−N3	86.58(10)
O7#2−Mn1−O2#3	86.36(10)	O8#2−Mn2−N3	91.12(11)
O7#1−Mn1−O2	86.36(10)	O1−Mn2−N1	175.41(10)
O7#2−Mn1−O2	93.64(10)	O8#2−Mn2−N1	87.01(10)
1			
3			
O2#3−Mn1−O2	180.000(1)	N3−Mn2−N1	92.90(11)
O7#1−Mn1−O5#3	85.74(9)	O1−Mn2−O5	91.92(8)
4			
Mn1−O8#1	2.079(4)	Mn1−O6	2.125(4)
Mn1−O1	2.124(4)	Mn1−O7#2	2.177(4)
Mn1−N4#3	2.198(4)	Mn2−O4#4	2.102(4)
Mn2−O2	2.143(4)	Mn2−O5	2.152(4)
Mn2−O3#5	2.166(4)	Mn2−N1	2.251(4)
Mn2−O9	2.411(3)	O4#4−Mn2−O2	164.86(16)
O8#1−Mn1−O6	144.58(16)	O8#1−Mn1−O1	93.70(16)
O8#1−Mn1−O7#2	86.67(16)	O6−Mn1−O7#2	84.64(14)
O1−Mn1−O7#2	179.45(16)	O8#1−Mn1−N4#3	107.03(16)
O6−Mn1−N4#3	106.75(16)	O1−Mn1−N4#3	93.12(16)
O7#2−Mn1−N4#3	87.16(15)	O6−Mn1−O1	94.82(14)
O4#4−Mn2−O5	89.67(17)	O2−Mn2−O5	91.46(15)
O4#4−Mn2−O3#5	87.07(16)	O2−Mn2−O3#5	91.25(15)
O5−Mn2−O3#5	176.34(16)	O4#4−Mn2−N1	98.06(17)
O2−Mn2−N1	96.92(17)	O5−Mn2−N1	93.97(17)
O3#5−Mn2−N1	88.14(16)	O4#4−Mn2−O9	90.06(14)
O2−Mn2−O9	74.85(14)	O5−Mn2−O9	89.82(13)
O3#5−Mn2−O9	88.52(12)	N1−Mn2−O9	171.05(14)
5			
Mn1−O1	2.051(2)	Mn1−O3#1	2.116(2)
Mn1−N1	2.221(3)	Mn1−O5	2.252(2)
Mn1−O8#2	2.309(2)	Mn2−O6	2.166(2)
Mn2−O6#3	2.166(2)	Mn2−O2	2.178(2)
Mn2−O2#3	2.178(2)	Mn2−O8#4	2.300(2)
Mn2−O8#2	2.300(2)	Mn3−O4#1	2.107(2)
Mn3−O5#6	2.205(2)	Mn3−O4#5	2.107(2)
Mn3−O7#2	2.248(2)	Mn3−O5	2.205(2)
Mn3−O7#3	2.248(2)	O1−Mn1−N1	93.37(11)
O1−Mn1−O3#1	94.16(10)	O1−Mn1−O5	116.59(10)
O3#1−Mn1−N1	88.04(10)	N1−Mn1−O5	149.97(10)
O3#1−Mn1−O5	87.81(8)	O6#3−Mn2−O2#3	95.52(9)
O6#3−Mn2−O6	85.59(13)	O6#3−Mn2−O2	167.74(8)
O6−Mn2−O2#3	167.74(8)	O2#3−Mn2−O2	86.00(13)
O6−Mn2−O2	95.52(9)	O4#1−Mn3−O5#6	97.21(9)
O4#1−Mn3−O4#5	90.96(14)	O4#1−Mn3−O5	88.29(9)
O4#5−Mn3−O5#6	88.29(9)	O5#6−Mn3−O5	172.18(11)

[a]Symmetry transformations used to generate equivalent atoms: #1: $x-{}^1/_2, -y+1, z-{}^1/_2$; #2: $-x+{}^3/_2, y+1, -z+{}^1/_2$ for **1**. #1: $x, y+1, z$; #2: $x, y-{}^1/_2, z+{}^1/_2$; #3: $-x+1, -y+{}^5/_2, z+{}^1/_2$; #4: $-x+1, -y+2, z$ for **2**. #1: $-x, -y, -z+1$; #2: $x+1, y, z$; #3: $-x+1, -y, -z+1$ for **3**. #1: $x, -y+2, z-{}^1/_2$; #2: $-x+1, -y+2, -z+2$; #3: $-x+{}^1/_2, y+{}^1/_2, -z+{}^3/_2$; #4: $x+{}^1/_2, -y+{}^3/_2, z+{}^1/_2$; #5: $-x+{}^1/_2, -y+{}^3/_2, -z+1$ for **4**. #1: $-x+{}^1/_2, -y+{}^1/_2, -z$; #2: $x+{}^1/_2, -y+{}^3/_4, -z+{}^1/_4$; #3: $-x+{}^1/_4, y, -z+{}^1/_4$; #4: $-x-{}^1/_4, -y+{}^3/_4, z$; #5: $x+{}^1/_4, y+{}^1/_4, -z$; #6 $-x+{}^3/_4, -y+{}^3/_4, z$ for **5**.

*$[Mn_3(tbip)_3(bix)_2]$ (**2**).* Compound **2** was synthesized in a similar way as that described for **1**, except that $Mn(OAc)_2{\cdot}4H_2O$ (0.2 mmol, 48.5 mg) is used. Colorless block crystals of **2** were obtained. Yield: 34.7 mg, 40% (based on Mn^{II}). Anal. (%) Calcd for $C_{64}H_{64}Mn_3N_8O_{12}$: C 59.04, H 4.95, N 8.61. Found: C 59.00, H 5.01, N 8.35. IR (cm^{-1}): 3126 m, 2965 m, 1624 s, 1575 s, 1547 s, 1429 s, 1371 s, 1360 s, 936 s, 865 s, 784 s, 775 s, 735 s, 728 s, 659 s.

*$[Mn_3(tbip)_2(Htbip)_2(bib)_2]{\cdot}4H_2O$ (**3**).* Compound **3** was synthesized in a similar way as that described for **1**, except that bix was replaced by bib (0.1 mmol, 19.0 mg). Colorless block crystals of **3** were obtained. Yield: 25.1 mg, 50% (based on Mn^{II}). Anal. (%) Calcd for $C_{68}H_{86}Mn_3N_8O_{20}$: C 54.44, H 5.78, N 7.47. Found: C 54.49, H 5.83, N 7.55. IR (cm^{-1}): 3149 m, 2963 m, 1706 m, 1608 s, 1580 s, 1478 s, 1412 s, 1379 s, 1235 s, 1086 m, 935 m, 781 s, 746 s, 679 s, 663 s.

*$[Mn_4(tbip)_4(bbp)_2(H_2O)_2]$ (**4**).* Compound **4** was synthesized in a similar way as that described for **1**, except that bix was replaced by bbp (0.1 mmol, 27.6 mg). Colorless block crystals of **4** were obtained. Yield: 20.2 mg, 48% (based on Mn^{II}). Anal. (%) Calcd for $C_{82}H_{82}Mn_4N_8O_{17}$: C 58.93, H 4.95, N 6.70. Found: C 58.99, H 5.00, N 6.67. IR (cm^{-1}): 2963 m, 1622 s, 1600 m, 1578 s, 1510 m, 1458 m, 1370 s, 1359 s, 1277 m, 910 m, 785 s, 738 s, 708 s, 697 m.

*$[Mn_4(tbip)_4(bip)]{\cdot}2H_2O$ (**5**).* Compound **5** was synthesized in a similar way as that described for **1**, except that bix was replaced by bip (0.1 mmol, 17.6 mg). Gray block crystals of **5** were obtained. Yield: 14.4 mg, 44% (based on Mn^{II}). Anal. (%) Calcd for $C_{57}H_{64}Mn_4N_4O_{18}$: C 52.15, H 4.91, N 4.27. Found: C 52.19, H 5.04, N 4.33. IR (cm^{-1}): 2966 m, 1600 m, 1597 m, 1540 s, 1518 m, 1430 s, 1415 s, 1371 s, 1309 m, 1271 m, 778 s, 735 s, 718 s, 660 s.

X-ray Crystallography. Single crystal X-ray diffraction data for complexes **1**−**5** were collected on a Bruker SMART APEX CCD diffractometer with graphite-monochromated Mo Kα radiation (λ = 0.710 73 Å) at room temperature. The structures were solved using direct methods and successive Fourier difference synthesis (SHELXS-97),[15] and

dx.doi.org/10.1021/ic3012537 | Inorg. Chem. 2012, 51, 9431−9442

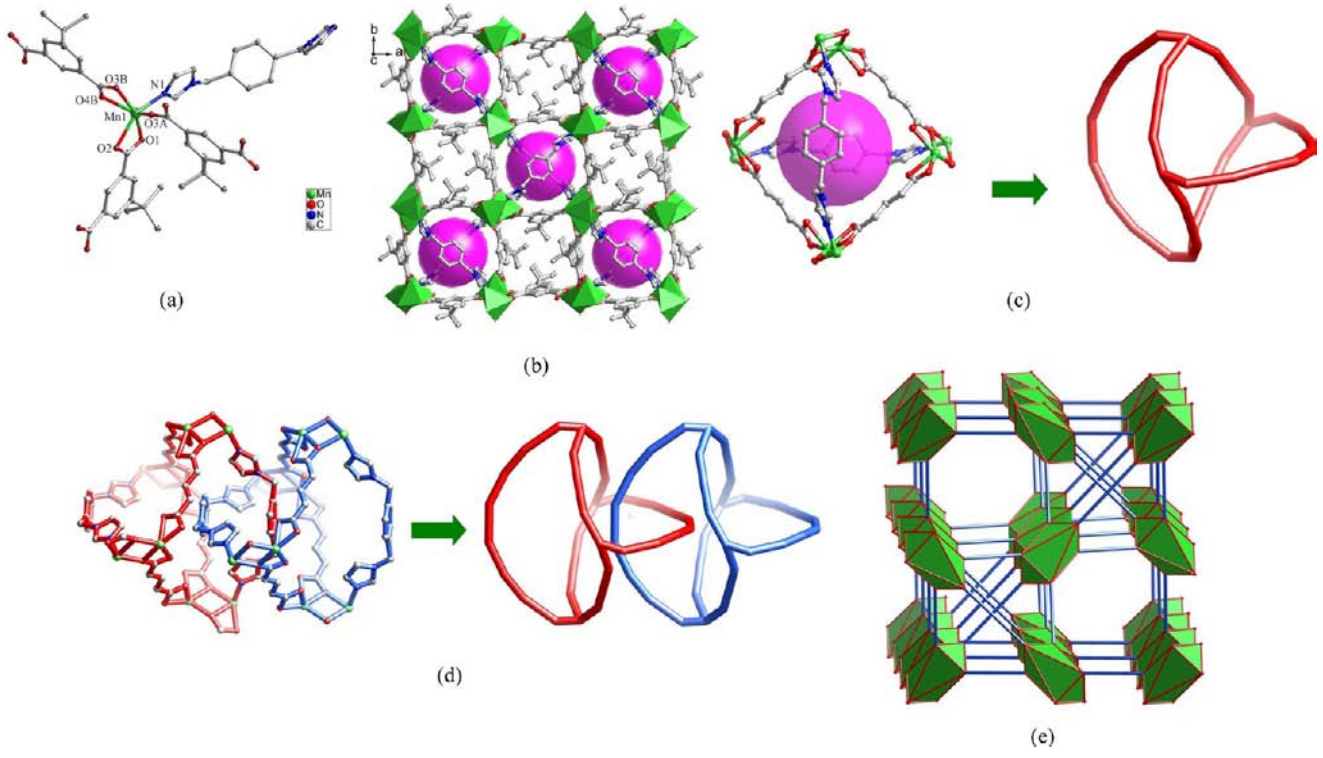

Figure 1. (a) Coordination environment of Mn^{II} ion in **1**. Symmetry codes for A: $x - {}^1/_2, -y + 1, z - {}^1/_2$. For B: $-x + {}^3/_2, y + 1, -z + {}^1/_2$. (b) View of 3D network of **1** containing two types of channels. (c) The cage-like unit in **1**. (d) The polycatenane character of **1**. (e) The augmented 6-connected net with the Schläfli symbol of $(3^6.6^6.7^3)$ (the vertices of the net are replaced by the flattened octahedra).

refined using the full-matrix least-squares method on F^2 with anisotropic thermal parameters for all non-H atoms (SHELXL-97).[15] The hydrogen atoms were assigned with common isotropic displacement factors and included in the final refinement with geometrical restraints. Further crystallographic data and selected bond parameters for **1**−**5** are listed in Tables 1 and 2. CCDC reference nos.: 881398 for **1**, 882893 for **2**, 881399 for **3**, 881400 for **4**, and 881401 for **5**.

RESULTS AND DISCUSSION

Description of Crystal Structures. *$[Mn_2(tbip)_2(bix)]$ (**1**).* As shown in Figure 1a, the asymmetric unit contains one tbip, one Mn^{II} ion, and a half bix molecule. The central Mn^{II} ion is six-coordinated with a distorted octahedral geometry by one nitrogen atom of bix and five carboxylic oxygen atoms from three tbip. The apical positions are occupied by one nitrogen atom (N1) of bix and one oxygen atom (O2) from tbip with the N1−Mn1−O2 angle of 149.18(6)°. The Mn−N length is 2.158(1) Å, and the Mn−O ones are in the range 2.128(1)−2.344(1) Å, respectively. The tbip ligand adopts μ_1-η^1:η^1-chelating and μ_2-η^2:η^1 coordinated modes for two carboxyl groups (Figure S1a, Supporting Information). Thus, two adjacent Mn^{II} ions are linked by two carboxylic oxygen atoms to form a $[Mn_2O_2]$ ring with the Mn···Mn distance of 3.42 Å, and the rings are connected by tbip to form a 3D framework with two types of channels (see Figure 1b). The tbip moieties protrude inside the voids of one type, and the other type is separated by bix, giving rise to individual molecular cages (Figure 1c,d). For each cage, four tbip link four binuclear Mn^{II} units to generate a twisty square, the diagonal of which is joined by two curving bix ligands.

In **1**, two identical 3D networks are mutually interpenetrated with each other to form a 2-fold parallel interpenetrating framework. However, due to the existence of cages, the overall structure not only shows a simple 2-fold interpenetration, and the most outstanding structural feature is the existence of polycatenane in such a 3D coordination polymer.

From the topological view, if one considered each binuclear Mn^{II} unit as a node, the 3D structure of **1** can be described as a 6-connected network with a new $(3^6.6^6.7^3)$ topology (Figure 1e). Obviously, this 3-D net is completely different from the most common *a*-polonium topology $(4^{12}.6^3)$ for the 6-connecting 3D frameworks, and other known but seldom observed 6-connecting nets such as $(4^8.5^4.6^3)$, $(4^8.5^3.6^4)$, $(4^9.6^6)$, and the binodal $(4^{12})(4^9.6^6)$ types.

Notably, when bipy, bpe, bpa, phen, or py (bipy = 4,4′-bipyridine, bpe = 1,2-bi(4-pyridyl)ethene, bpa = 1,2-bi(4-pyridyl)-ethane, phen = phenanthroline, py = pyridine) and Mn^{II} are used as the starting materials, $[Mn(tbip)(bipy)]_n$ (**6**),[14a] $\{[Mn(tbip)(bpe)]\cdot 1.5H_2O\}_n$ (**7**),[14a] $[Mn(tbip)(bpa)]_n$ (**8**),[14a] $\{[Mn_2(tbip)_2(phen)_2]\cdot 2H_2O\}_n$ (**9**),[16] and $[Mn(tbip)(py)_2]_n$ (**10**),[17] with dinuclear $[Mn(COO)]_2$ units can be obtained. Though tbip has similar coordination modes (μ_2-η^1:η^1/μ_1-η^1:η^1) in **6**, **7**, **8**, **9**, and **10**, different network structures are observed, that is, a 3D (3,5)-connected net with a $(4.6.8)(4.6_5.8_3.10)$ topology of **6**, a 3D layer-pillar framework of **7**, a 2D layer of **8**, a 1D chain of **9**, and a 2D (4,4) layer of **10**. This structural difference can be ascribed to the different N-containing ligands therein.

*$[Mn_3(tbip)_3(bix)_2]$ (**2**).* Crystal structure analysis reveals that the asymmetric unit of **2** consists of 1.5 Mn^{II} ions, 1.5 tbip, and one bix. The coordination environments around the Mn^{II} centers are represented in Figure 2a. A trinuclear $[Mn_3(COO)_6]$ SBU is formed, in which two adjacent Mn(II) ions are bridged by two tbip with the Mn1···Mn2 distance of 3.66 Å and the Mn2···Mn1···Mn2A angle of 172.5°. The Mn1 center takes a distorted octahedral geometry, provided by four O atoms from three tbip and two nitrogen atoms from two bix. The Mn2 center

dx.doi.org/10.1021/ic3012537 | Inorg. Chem. 2012, 51, 9431−9442

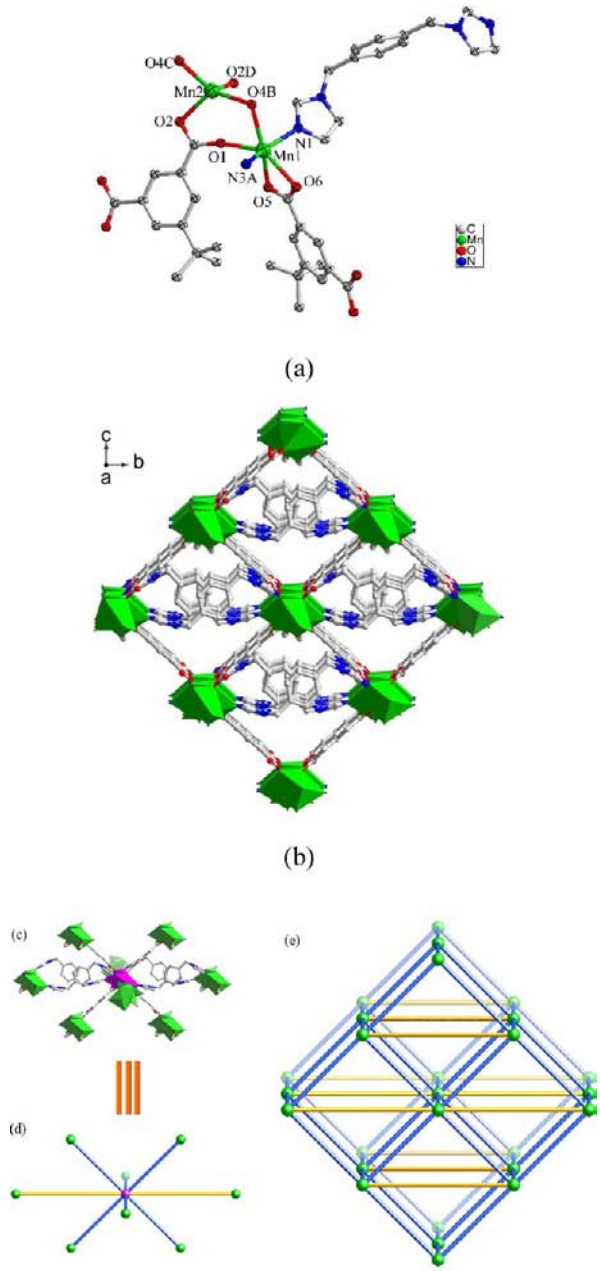

Figure 2. (a) Coordination environments of Mn^{II} ions in **2**. Symmetry codes for A: $x, y + 1, z$. B: $x, y - {}^{1}/_{2}, z + {}^{1}/_{2}$. C: $-x + 1, -y + {}^{5}/_{2}, z + {}^{1}/_{2}$. D: $-x + 1, -y + 2, z$. (b) The 3D network of **2** viewing along the [100] direction. (c and d) A schematic representation of the connectivity of a net node. (e) The $(3^6.4^{18}.5^3.6)$ topological network (the trinuclear Mn^{II} clusters are represented by green balls).

is four coordinated by four oxygen atoms from four tbip. The Mn−N bond lengths are 2.197(3) and 2.211(3) Å, and the Mn−O bond lengths are in the range 2.144(3)−2.306(2) Å, respectively. The tbip in **2** shows two kinds of coordinated modes (μ_2-tbip and μ_4-tbip; see Figure S1b,c, respectively). The trinuclear $[Mn_3(COO)_6]$ SBUs are linked in sequence by the carboxyl groups of μ_2-tbip (μ_1-η^1:η^1 for both carboxyl groups) to form an infinite chain along the *a* axis. Each chain is linked to four adjacent chains through the μ_4-tbip (μ_2-η^1:η^1 and μ_2-η^0:η^2 coordinated mode for two carboxyl groups) to generate a 3D framework with pcu topology (Figure S2, Supporting Information). In addition, paired bix ligands link the chains within the above pcu network to build a complicated 3D framework (Figure 2b). From the topological point of view, each trinuclear $[Mn_3(COO)_6]$ SBU is linked to eight SBUs (Figure 2c and 2d) by tbip and bix ligands, constructing an 8-connected hex net with the Schläfli symbol of $(3^6.4^{18}.5^3.6)$ (Figure 2e).

$[Mn_3(tbip)_2(Htbip)_2(bib)_2]\cdot 4H_2O$ (***3***). The structure of **3** possesses a 3D network based on the linear trimetallic $[Mn_3(COO)_6]$ clusters. The six-coordinated Mn2, Mn1, and Mn2A (A = $-x + 1, -y, -z + 1$) centers are bridged through six carboxyl groups to form a corner-sharing trinuclear unit, in which the Mn1···Mn2 distance is 3.66 Å. The Mn1 atom lies on an inversion center. As shown in Figure 3a, there are two crystallographically independent Mn^{II} ions in **3**. Mn1 is coordinated by six oxygen atoms from four tbip and two Htbip to finish a distorted octahedral geometry. The Mn2 atom is six coordinated by three oxygen atoms from two tbip, one oxygen atom from one Htbip, and two nitrogen atoms from two bib. The Mn−N bond lengths are 2.223(3) and 2.257(3) Å, and the Mn−O ones are in the range 2.098(2)−2.334(2) Å. In **3**, the tbip acts as a tetradentate ligand with μ_2-η^1:η^1 and μ_2-η^1:η^2 coordinated modes for two carboxyl groups (see Figure S1d, Supporting Information), and the carboxyl group of Htbip adopts a μ_2-η^1:η^1 coordinated mode (see Figure S1e, Supporting Information).

It is worth noting that the adjacent trinuclear subunits are connected by tbip to form a 1D chain decorated with Htbip at two sides in an outward fashion (see Figure 3b). These 1D chains are interconnected by the bib spacers to afford a 3D framework (see Figure 3c). From a topological perspective, if one considers the trinuclear cluster as a node, the 3D network can be described as a familiar 6-connected pcu topology (see Figure 3d).

Two Mn^{II}-tbip coordination polymers with linear $[Mn_3(COO)_6]$ trinuclear units have been reported, namely $[Mn_3(tbip)_3(bpy)_2]_n$ (**11**)[16] and $[Mn_3(tbip)_2(Htbip)_2((CH_3)_2CHOH)_2]$ (**12**)[10] (bpy = 2,2′-bipyridine) that show 2D layer structures. The coordination modes of tbip/Htbip in **12** are similar to those in **3**, while those of tbip in **11** (μ_2-η^1:η^2/μ_2-η^1:η^2) are different. These results reveal that the auxiliary bib ligand plays a fatal role in the structure of **3**.

$[Mn_4(tbip)_4(bbp)_2(H_2O)_2]$ (***4***). Crystal structure analysis reveals that the asymmetric unit of **4** consists of two Mn^{II} centers, two tbip, one bbp, and one coordinated water. As shown in Figure 4a, the Mn1 center is five-coordinated with a distorted square-pyramidal geometry, in which four O atoms from four tbip (O1, O6, O8A, and O7B, symmetry code A: $x, -y + 2, z - {}^{1}/_{2}$. B: $-x + 1, -y + 2, -z + 2$.) form the equatorial plane, and the vertex is occupied by one N atom (N4C, symmetry code C: $-x + {}^{1}/_{2}, y + {}^{1}/_{2}, -z + {}^{3}/_{2}$) from bbp. The Mn2 ion takes a distorted octahedral geometry, in which two O atoms (O2 and O4D, symmetry code D: $x + {}^{1}/_{2}, -y + {}^{3}/_{2}, z + {}^{1}/_{2}$) from two tbip and one O atom from a coordinated water molecule form the equatorial plane and the apical positions are occupied by two O atoms (O5 and O3E, symmetry code E: $-x + {}^{1}/_{2}, -y + {}^{3}/_{2}, -z + 1$) from another two tbip. The Mn−N bond lengths are 2.198(4) and 2.251(4) Å, and the Mn−O ones are in the range 2.079(4)−2.411(3) Å. Each Mn1 ion is linked to the adjacent Mn^{II} ions *via* two carboxyl groups, and each Mn2 center is linked to one adjacent Mn2 *via* two carboxyl and one μ_2-H_2O as well as one adjacent Mn1 ion *via* two carboxyl groups, forming a tetranuclear $[Mn_4(\mu_2\text{-}COO)_8(\mu_2\text{-}H_2O)]$ unit (Figure S3, Supporting Information) with the Mn···Mn distances of 3.959(2), 4.292(2), 4.781(2), and

dx.doi.org/10.1021/ic3012537 | *Inorg. Chem.* 2012, 51, 9431−9442

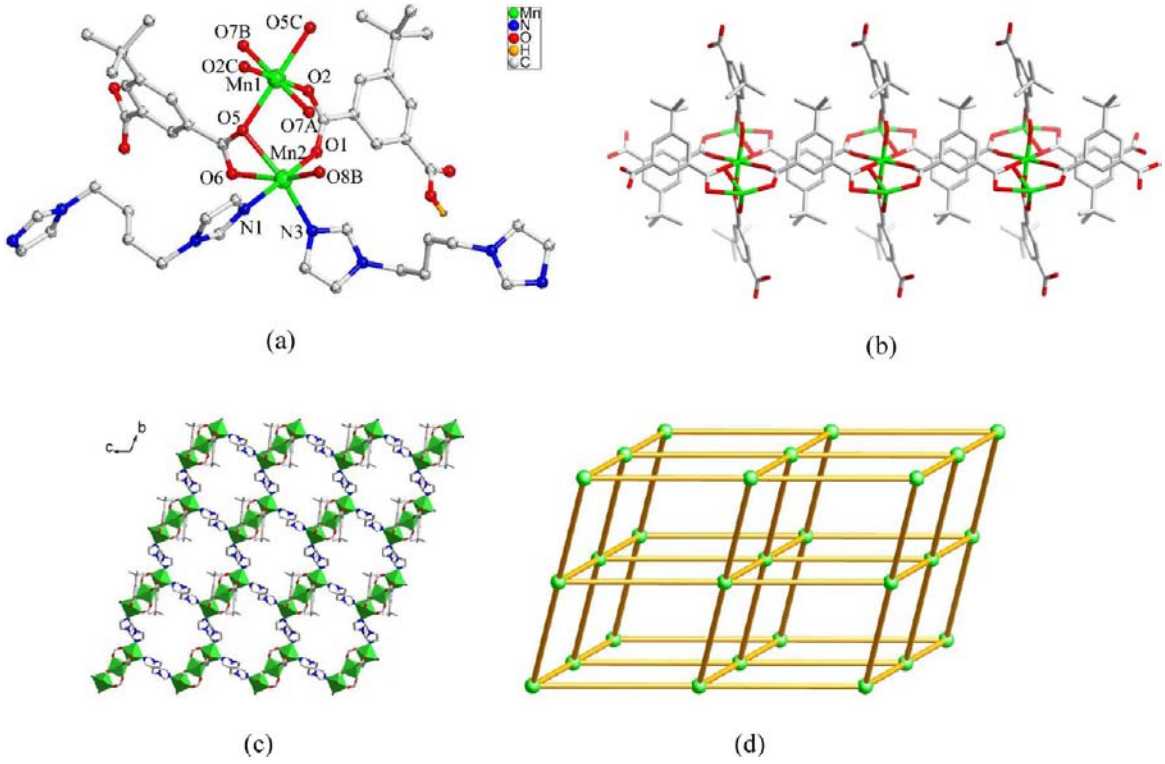

Figure 3. (a) Coordination environments of Mn^{II} ions in **3**. Symmetry codes for A: $-x, -y, -z + 1$. B: $x + 1, y, z$. C: $-x + 1, -y, -z + 1$. (b) The 1D chain constructed by tbip, Htbip, and Mn^{II} ions along the *a* axis. (c) The 3D network of **3** viewing along [100]. (d) Schematic representation of the pcu topology (the trinuclear Mn^{II} clusters are represented by green balls).

4.781(2) Å. The tbip in **4** shows a μ_4 (μ_2-η^1:η^1 for both carboxyl groups) coordinated mode (see Figure S1f, Supporting Information). Each tetranuclear unit is further linked to four neighboring tetranuclear units through eight tbip in a double-bridge fashion and another four neighboring units through four bbp, resulting in a 3D open framework (Figure 4b). The overall structure of **4** can be described as a 8-connected network with $[Mn_4(\mu_2\text{-}COO)_8(\mu_2\text{-}H_2O)]$ SBUs as nodes (Figure 4c,d) with the Schläfli symbol of $(3^6.4^{16}.5^6)$, as shown in Figure 4e.

*$[Mn_4(tbip)_4(bip)]\cdot 2H_2O$ (**5**).* There are three crystallographically independent Mn^{II} ions in **5** (Figure 5a). Mn1 has a slightly distorted square-pyramidal geometry, formed by four oxygen atoms from four tbip, and one nitrogen atom from one bip. Both Mn2 and Mn3 ions show the distorted octahedral geometry, defined by six oxygen atoms from different tbip ligands. The Mn−N bond length is 2.221(3) Å, and the Mn−O ones are in the range 2.051(2)−2.486(2) Å. The Mn1···Mn2 and Mn1···Mn3 distances are 3.55 and 3.20 Å, and the Mn2···Mn1···Mn3, Mn1A···Mn2···Mn1, and Mn1···Mn3···Mn1B (symmetry codes: A, $-x + 0.25, y, -z + 0.25$; B, $-x + 0.75, -y + 0.75, z$) angles are 110.3°, 165.5°, and 170.5°, respectively. The Mn1···Mn2 and Mn1···Mn3 distances here are similar to those in $[Mn_4(tbip)_4(CH_3OH)_2]\cdot 2H_2O$ (**13**).[10] The tbip ligand shows two kinds of coordinated modes (μ_2-η^1:η^1 for both carboxyl groups of μ_4-tbip, and μ_3-η^1:η^2 coordinated mode for both carboxyl groups of μ_6-tbip; see Figure S1f,g, Supporting Information). The carboxyl groups (μ_4- and μ_6-tbip) bridge the Mn^{II} ions to form a 4_1 helical chain along [100] with the pitch of 11.61 Å (see Figure 5b). Each helical chain is further interconnected to four neighboring helices with opposite chirality *via* μ_4-tbip linkers in double-bridge fashion, leading to the formation of a 3D framework (see Figure 5c), where each bip acts as a bridging ligand dangling on two sides of the helical chain.

From the topological point of view, each μ_4-tbip ligand can be viewed as a four-connected node, each Mn1 center as a 5-connected node, as well as each μ_6-tbip, Mn2, or Mn3 as a 6-connected node, resulting in the final 3D net with a (4,5,6)-connected $(4^3.6^2.8)_2(4^6.5^3.7)_2(4^9.5^2.6^4)_2(4^9.5^3.6^2.7)(4^9.6^5.8)$ topology, as shown in Figure 5d.

Synthetic Chemistry and Structural Diversity. In this work, coordination polymers **1**−**5** were isolated under the same hydrothermal conditions. Compounds **1**−**5** are air stable and insoluble in common organic solvents, and can retain their crystalline integrity at ambient condition for a long time. No characteristic absorption band of −COOH (at 1700−1750 cm^{-1}) is observed from the IR spectra of **1**, **2**, **4**, and **5**, which indicates that the carboxylic groups of ligands therein are completely deprotonated. In contrast, the H_2tbip ligands in **3** display different degrees of deprotonation with both Htbip and tbip existing.[18] The synthetic route for the Mn^{II}−H_2tbip/bix, bib, bbp, bip system is schematically depicted in Scheme 1.

Compared with the crystal structures of **1**−**5**, it can be concluded that the coordination geometry of Mn^{II} and coordination fashion of tbip will play a key role in constructing their lattice architectures. The Mn^{II} centers in **1**−**5** can adopt a variety of coordination environments such as $[MnO_5N]$, $[MnO_6]$, $[MnO_4N_2]$, and $[MnO_4N]$. Meanwhile, the tbip ligands take different bridging modes such as μ_2-, μ_3-, μ_4-, and μ_6-fashions to connect the Mn^{II} ions. As a result, the Mn^{II} centers in **1**−**5** can be extended in different ways to form various network structures.

dx.doi.org/10.1021/ic3012537 | *Inorg. Chem.* 2012, 51, 9431−9442

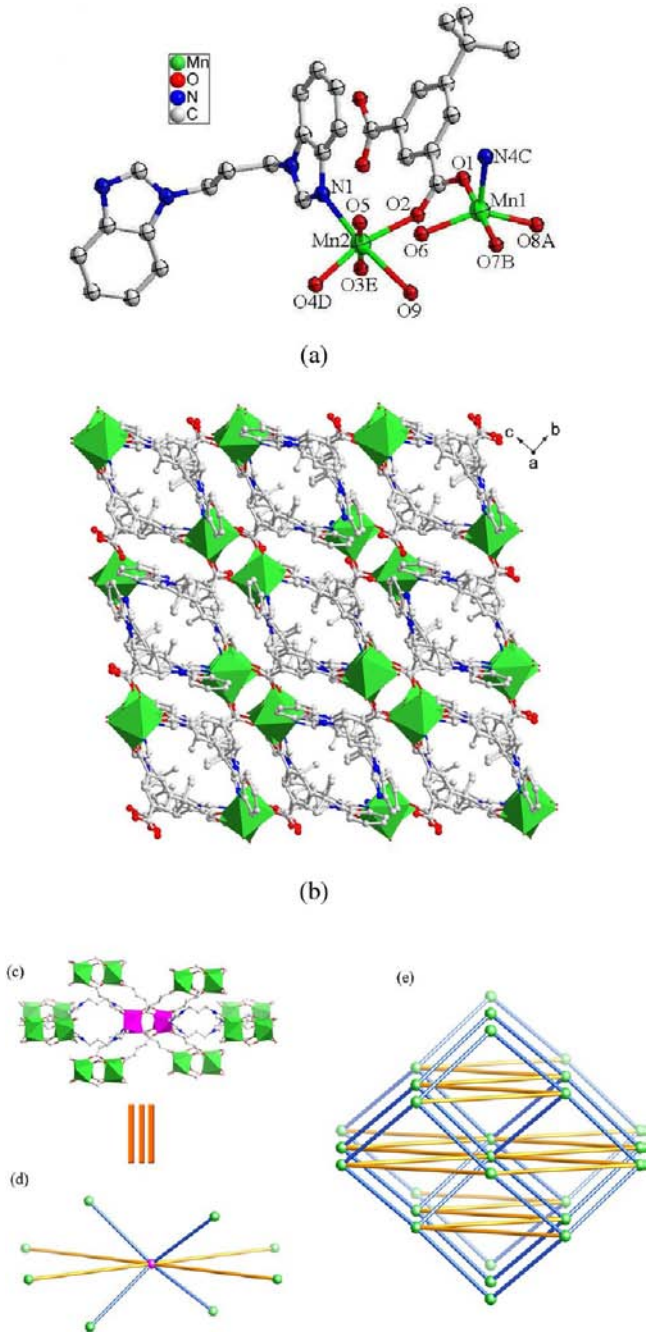

Figure 4. (a) Coordination environments of Mn^{II} ions in **4**. Symmetry codes for A: $x, -y + 2, z - {}^1/_2$. B: $-x + 1, -y + 2, -z + 2$. C: $-x + {}^1/_2, y + {}^1/_2, -z + {}^3/_2$. D: $x + {}^1/_2, -y + {}^3/_2, z + {}^1/_2$. E: $-x + {}^1/_2, -y + {}^3/_2, -z + 1$. (b) The 3D network of **4** viewing along [100]. (c and d) Schematic representation of the connectivity of one network node. (e) The $(3^6.4^{16}.5^6)$ topological network (the tetranuclear Mn^{II} units are represented by green balls).

On the other hand, the molar ration of the reactants and the auxiliary N-donor ligands also play an important role in governing the coordination motifs and the final supramolecular structures. Taking the bix ancillary into account, complexes **1** and **2** are synthesized in similar synthetic conditions. The difference of molar ration of the reactants for the synthesis of **1** and **2** is a sole determining factor that dominates their distinct structures. Although complexes **1** and **3**–**5** were prepared under similar hydrothermal conditions, they show completely different 3D coordination frameworks due to the presence of various N-donor ligands.

PXRD and TGA Results. In order to check the phase purity of the complexes, powder X-ray diffraction (PXRD) patterns of **1**–**5** were recorded at room temperature. As shown in Figure S4, Supporting Information, the peak positions of the simulated and experimental PXRD patterns are in agreement with each other, which confirm their phase purity. The difference in intensity of some diffraction peaks may be attributed to the preferred orientation of the crystalline powder samples.

In order to characterize the complexes more fully in terms of thermal stability, their thermal behaviors were studied by thermogravimetric analysis (TGA) in a dry nitrogen atmosphere from 30 to 900 °C. The experiments were performed on samples consisting of numerous single crystals of **1**–**5** (see Figure S5, Supporting Information). For complex **1**, the framework collapses in the temperature range 205–900 °C before the final formation of metal oxide. For **2**, the framework begins to collapse at 395 °C, which indicates that the framework is thermally stable over a wide range of temperature, and the observed weight losses including two steps between 395 and 900 °C before the final formation of metal oxide can be assigned to the elimination of organic ligands. Complex **3** loses the lattice water molecules at 90–115 °C (calcd 4.8% and expt 4.7%). Above this temperature to 230 °C, there is no further weight loss, which indicates that the dehydrated framework is thermally stable over a wide range of temperature. The remaining weight of 13.2% indicates that the final product is MnO (14.2% calcd). Complex **4** loses the coordinated water molecules at 245–317 °C (calcd 2.2% and expt 2.8%), and the residue remains unchanged until 430 °C, whereupon expulsion of its organic components occurs. The final mass remnant of 17.2% at 595 °C likely represents the deposition of MnO (17.0% calcd). Complex **5** loses its coordinated water molecules in 155–350 °C (calcd 2.2% and expt 2.5%), and then, pyrolysis of the sample occurs with two steps of weight loss.

Magnetic Properties. The magnetic susceptibilities, χ_M's, of **1**–**5** were measured in the temperature range 2–300 K at 2000 G. For complex **1**, the experimental $\chi_M T$ value at 300 K is 8.17 $cm^3\ mol^{-1}$ K, which is lower than that expected for a noninteracting pair of $S = {}^5/_2$ ions (8.75 $cm^3\ mol^{-1}$ K) (Figure 6). As temperature lowers to 2 K, the $\chi_M T$ value decreases first slowly and then rapidly. This behavior suggests that antiferromagnetic interactions are operative in **1**. The temperature dependence of the reciprocal susceptibilities ($1/\chi_M$) obeys the Curie–Weiss law above 10 K with a Weiss constant $\theta = -5.57$ K, Curie constant $C = 8.45$ $cm^3\ K\ mol^{-1}$, and $R = 8.59 \times 10^{-5}$. The negative θ value also reveals the presence of antiferromagnetic interactions in **1**.

To quantitatively evaluate the magnetic interactions in **1**, for similar binuclear Mn^{II} complexes, the following eq 1 is induced using a Dirac–van Vleck–Heisenberg spin Hamiltonian $\hat{H} = -2J\hat{S}_1 \cdot \hat{S}_2$.[14a,19]

$$X_M = 2\frac{Ng^2\beta^2}{kT}\frac{A}{B} \qquad (1)$$

The least-squares analysis of magnetic susceptibilities data leads to $J = -1.08$ cm^{-1}, $g = 1.96$, and $R = 1.18 \times 10^{-4}$ (the agreement factor $R = \sum[(\chi_M)_{obs} - (\chi_M)_{calc}]^2/\sum[(\chi_M)_{obs}]^2$).

dx.doi.org/10.1021/ic3012537 | Inorg. Chem. 2012, 51, 9431–9442

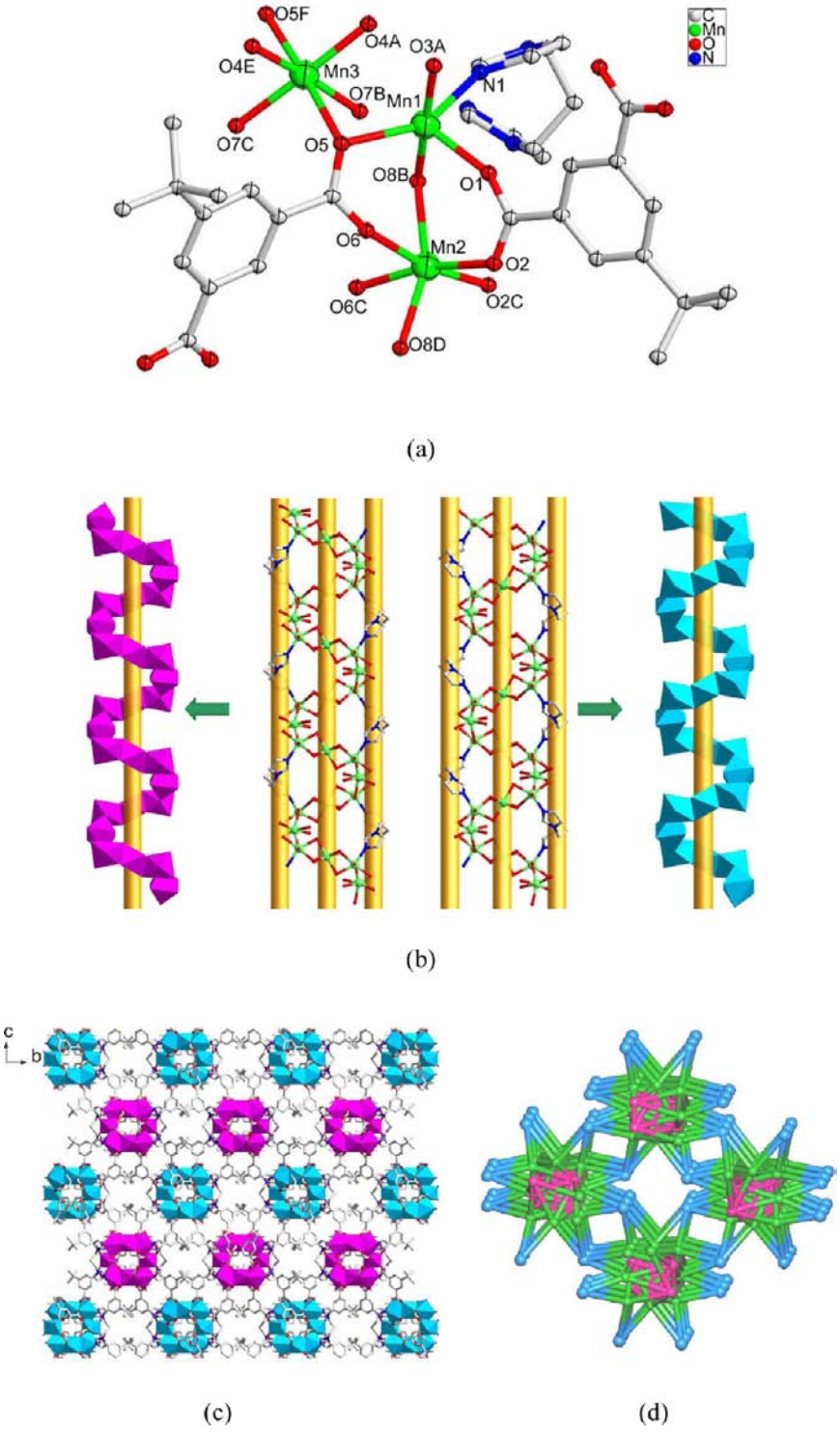

Figure 5. (a) Coordination environments of Mn^{II} ions in **5**. Symmetry codes for A: $-x + {}^{1}/_{2}, -y + {}^{1}/_{2}, -z$. B: $x + {}^{1}/_{2}, -y + {}^{3}/_{4}, -z + {}^{1}/_{4}$. C: $-x + {}^{1}/_{4}, y, -z + {}^{1}/_{4}$. D: $-x - {}^{1}/_{4}, -y + {}^{3}/_{4}, z$. E: $x + {}^{1}/_{4}, y + {}^{1}/_{4}, -z$; F: $-x + {}^{3}/_{4}, -y + {}^{3}/_{4}, z$. (b) Polyhedral view of the left- and right-handed helical chains. (c) The 3D network of **5** viewing along [100]. (d) Schematic representation of (4,5,6)-connected $(4^3.6^2.8)_2(4^6.5^3.7)_2(4^9.5^2.6^4)_2(4^9.5^3.6^2.7)$-$(4^9.6^5.8)$ topological net (blue balls for μ_4-tbip, violet balls for μ_6-tbip, and green balls for Mn^{II}).

The negative J value suggests that weak antiferromagnetic interactions between the adjacent Mn^{II} ions are mediated. Field-cooled magnetic susceptibility at a field of 2000 Oe (see Figure S6, Supporting Information) shows there is no apex in the plot, suggesting impossible spin-glass or superparamagnetic behavior.

For **2** and **3**, the observed $\chi_M T$ values at 300 K are 13.05 (see Figure 7) and 12.70 $cm^3\ mol^{-1}\ K$ (see Figure 8), respectively, which are slightly lower than the spin-only value (13.13 $cm^3\ mol^{-1}\ K$) expected for three uncoupled high-spin Mn^{II} ions. As the sample is cooled from room temperature, the $\chi_M T$ values increase up to the maximum of 18.25 $cm^3\ mol^{-1}\ K$ at 2 K for **2** while those decrease first slowly and then rapidly for **3**. The magnetic susceptibilities data in 10−300 K can be well fitted to the Curie−Weiss law with a Weiss constant θ = 2.11 K, Curie

dx.doi.org/10.1021/ic3012537 | Inorg. Chem. 2012, 51, 9431−9442

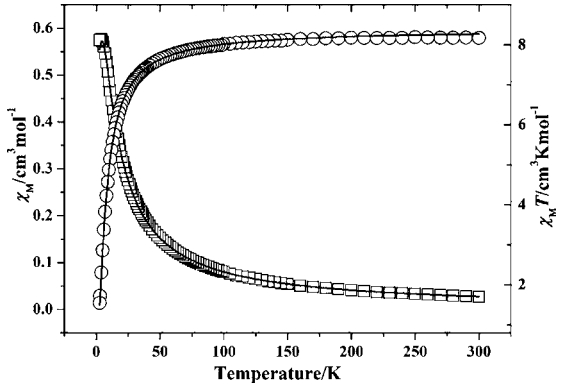

Figure 6. Temperature dependence of $\chi_M T$ and χ_M versus T for **1**. Open circles are the experimental data and the solid line represents the best fit obtained from the Hamiltonian given in the text.

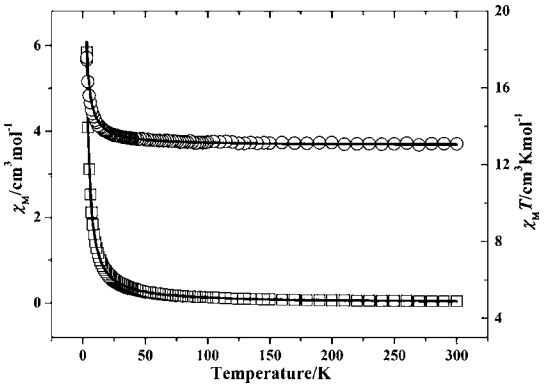

Figure 7. Temperature dependence of $\chi_M T$ and χ_M versus T for **2**. Open circles are the experimental data, and the solid line represents the best fit obtained from the Hamiltonian given in the text.

constant C = 13.0 cm^3 K mol^{-1}, and $R = 7.72 \times 10^{-5}$ for **2** and $\theta = -13.2$ K, C = 13.2 cm^3 K mol^{-1}, and $R = 5.27 \times 10^{-5}$ for **3**. The magnetic behavior and the θ value suggest that ferromagnetic interactions are operative in **2** while antiferromagnetic interactions are operative in **3**.

According to the structures of **2** and **3**, it could be presumed that the main magnetic interactions between the Mn^{II} centers should happen between the intracluster units through the short carboxylate bridges whereas the superexchange interactions between the Mn^{II} ions through tbip and bib can be ignored because of the long distances of Mn···Mn separations (greater than 9.6 Å). Thus, it is possible to interpret the observed magnetic behavior by using a modified analytical expression (eq 2[13c,20]) derived by combining the linear trinuclear Mn^{II} model [$\hat{H} = -J(\hat{S}_1 \cdot \hat{S}_2 + \hat{S}_2 \cdot \hat{S}_3)$],

$$X_M = \frac{Ng^2\beta^2}{3kT}\frac{C}{D} \qquad (2)$$

The least-squares analysis of magnetic susceptibilities data leads to J = 0.10 cm^{-1}, g = 1.99, and $R = 1.49 \times 10^{-4}$ for **2** and J = −0.92 cm^{-1}, g = 2.00, and $R = 1.61 \times 10^{-4}$ for **3**. The small J value indicates weak ferromagnetic interactions between the carboxylate bridged Mn^{II} ions in **2** and antiferromagnetic interactions between the Mn^{II} ions in **3**.

For complex **4**, the experimental $\chi_M T$ value at 300 K is 17.1 cm^3 mol^{-1} K, being close to that expected for four uncoupled high-spin Mn^{II} ions (17.5 cm^3 mol^{-1} K) (Figure 9). As the temperature is lowered, the $\chi_M T$ value decreases continuously, and the χ value first increases to a maximum at 10 K and then decreases. Above 10 K, a typical paramagnetic Curie−Weiss behavior is observed, with a Weiss constant θ = −14.4 K, Curie constant C = 17.98 cm^3 K mol^{-1}, and $R = 8.69 \times 10^{-5}$, respectively. The negative θ value and the decrease of $\chi_M T$ are indicative of antiferromagnetic interactions in **4**.

In **4**, the main magnetic interactions may be considered to occur in the tetranuclear [$Mn_4(COO)_8(H_2O)$] units linked by carboxylate groups and water molecules, whereas the exchange interactions between Mn(II) ions bridged through the tbip or bbp can be ignored because of the long Mn···Mn separations. Thus, an attempt was made to fit the magnetic susceptibility data, assuming that the carboxylate groups and water molecules bridge the Mn(II) ions to form a discrete tetranuclear unit. Four intracluster Mn···Mn interactions are 3.959(2), 4.292(2), 4.781(2), and 4.781(2) Å, and the exchange angles are 87.9(2)° and 91.8(2)°, respectively. Attempts were made to fit the

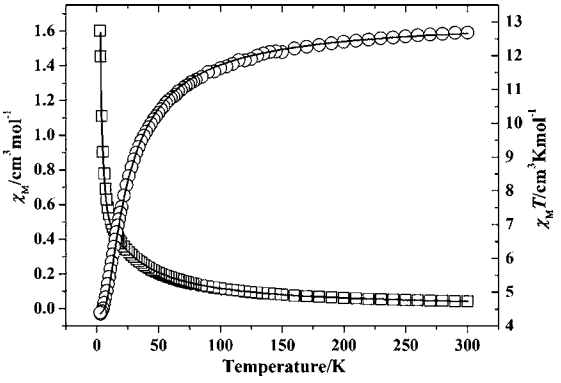

Figure 8. Temperature dependence of $\chi_M T$ and χ_M versus T for **3**. Open circles are the experimental data, and the solid line represents the best fit obtained from the Hamiltonian given in the text.

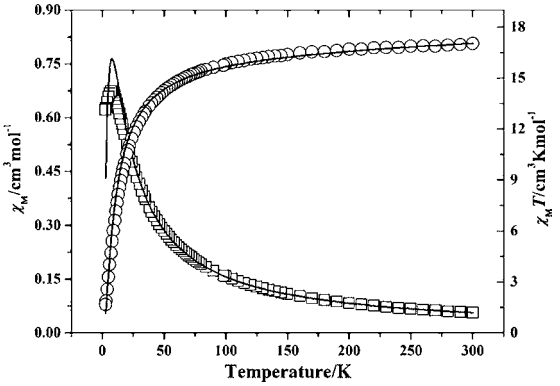

Figure 9. Temperature dependence of $\chi_M T$ and χ_M versus T for **4**. Open circles are the experimental data, and the solid line represents the best fit obtained from the Hamiltonian given in the text.

magnetic susceptibility data using a two or three or four J model. However, a satisfactory fit could not be achieved to describe the magnetic coupling between the Mn^{II} ions. In order to fit the magnetic susceptibility data, a simple model with only one J model was initially assumed. The analytical expression (eq 3) derived by Curély for a square lattice of classical spins[21] is given here.

$$X_M = [Ng^2\beta^2 S(S+1)(1+u^2)]/[3kT(1-u^2)] \qquad (3)$$

dx.doi.org/10.1021/ic3012537 | Inorg. Chem. 2012, 51, 9431−9442

Here $S = {}^5/_2$, and u is the well-known Langevin function, $u = \coth[JS(S+1)/kT] - kT/JS(S+1)$. The best fit leads to $J = -0.49$ cm^{-1}, $g = 2.26$, and $R = 5.824 \times 10^{-4}$. The small negative J value corroborates the presence of weak antiferromagnetic interactions between Mn^{II} ions through the carboxylate bridges. Gao et al. have also reported the magnetic properties of a Mn^{II} complex containing square Mn$_4$ units ($J = -0.45$ cm^{-1} and $g = 2.0$).[22] Field-cooled magnetic susceptibility at a field of 2000 Oe (see Figure S7, Supporting Information) shows that there is no apex in the plot, suggesting impossible spin-glass or superparamagnetic behavior.

For complex **5**, the experimental $\chi_M T$ value at room temperature is 3.67 cm^3 mol^{-1} K (Figure 10), which is lower

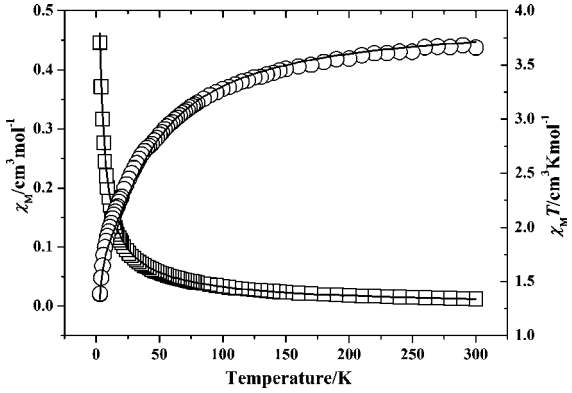

Figure 10. Temperature dependence of $\chi_M T$ and χ_M versus T for **5**. Open circles are the experimental data, and the solid line represents the best fit obtained from the Hamiltonian given in the text.

than the spin-only value (4.38 cm^3 mol^{-1} K) expected for a magnetically isolated high-spin Mn^{II} ion. As the temperature lowers, the $\chi_M T$ values decrease gradually. In the temperature region above 15 K, a typical paramagnetic Curie–Weiss behavior is observed, with a Weiss constant $\theta = -15.5$ K, Curie constant $C = 3.86$ cm^3 K mol^{-1}, and $R = 1.82 \times 10^{-4}$, respectively. The negative θ value and the decrease of the $\chi_M T$ are indicative of antiferromagnetic interactions in **5**.

The 3D structure of **5** was constructed by using tbip to link the 1D chains formed through carboxylate, carboxyl oxygen, and bip. Normally, very weak coupling can be conducted through tbip or bip, and thus, the magnetic behaviors show the character of 1D chain. The coupling transferred by two carboxylate between Mn2 and Mn3, which is weaker than that mediated by two carboxylate and oxygen atoms between Mn1 and Mn2, can be neglected. This is due to the longer distance between Mn2 and Mn3 and the *syn–anti* bridge with an additional high torsion (O5–C19–O6 and O7–C19–O8). Thus, the chain can be seen as a 1D system with two structurally different sets of triple bridges alternating in an AABB sequence. Thus, the magnetic exchange pathway within the helical chain can be described as a Mn^{II} chain with periodic $-J_1J_1J_2J_2-$ coupling sequence. In recent papers, Bu et al.,[23] Gao et al.,[24] and Du et al.[10] have also reported such a sequence. The values of J_1 and J_2 reported by Bu and Gao are negative with an antiferromagnetic state, while the values of J_1 and J_2 reported by Du are opposite with a ferromagnetic state, where the ferromagnetic exchange coupling may be due to the different coordinated mode of carboxyl group. In order to evaluate the interaction, the least-squares fit of magnetic data using the theoretical expression proposed by Fisher[25] and extended by Abu-Youssef[26] and others[23,24] was made. The spin Hamiltonian of an alternating $-J_1J_1J_2J_2-$ coupling sequence is

$$\hat{H} = \sum (J_1 S_{4i+1} S_{4i+2} + J_1 S_{4i+2} S_{4i+3} + J_2 S_{4i+3} S_{4i+4} + J_2 S_{4i+4} S_{4i+5})$$

The magnetic susceptibility is given by eq 4.

$$X_M = \frac{Ng^2\beta^2 S(S+1)}{12kT} \frac{A}{1 - u_1^2 u_2^2} \quad (4)$$

$$A = 4 + 4u_1 + 4u_2 + 4u_1u_2 + 2u_1^2 + 2u_2^2 + 4u_1^2u_2 + 4u_1u_2^2 + 4u_1^2u_2^2$$

Here, $S = {}^5/_2$, and u is the well-known Langevin function, $u = \coth[JS(S+1)/kT] - kT/JS(S+1)$. The best fit leads to $J_1 = -4.15$ cm^{-1}, $J_2 = -0.15$ cm^{-1}, $g = 1.90$, and $R = 6.622 \times 10^{-4}$. The negative J_1 and J_2 values confirm that slightly different magnetic exchanges are mediated through the alternant triple bridges, which indicate the antiferromagnetic interactions between the Mn^{II} ions.

Among the superexchange pathways between the nearest neighboring Mn^{II} ions, ferro- or antiferromagnetic couplings occur depending on the different carboxylate bridging modes.[10] According to Goodenough's rules, the μ_2-O bridges can mediate ferromagnetic couplings, as the corresponding Mn–O–Mn angles (87.97–100.69°) are within the range expected for a ferromagnetic interaction.[27] On the other hand, it can be speculated that the exchange interaction between two Mn^{II} ions bridged by the double *syn–syn* carboxylate bridges is dominantly antiferromagnetic,[13c,14,28] and that bridged by the *syn–anti* carboxylate bridges is ferromagnetic.[29] In **1**, the antiferromagnetic interactions between Mn^{II} ions may be due to the larger Mn1–O3A–Mn1C and Mn1–O3B–Mn1C (symmetry code C: $-x+2, -y+1, -z$) angles (103.3°).[30] The J value for **1** is also reasonable considering that Mn^{II} ions in a bis(μ_2-O) unit are generally weakly coupled, either antiferromagnetically[31] or ferromagnetically.[32] There are two factors that could affect the magnetic properties: the electronic effects due to the different carboxylate bridge and the structural parameters. Though **2**, **3**, and **12** all have trinuclear Mn^{II} units, **2** and [Mn$_3$(tbip)$_2$(Htbip)$_2$((CH$_3$)$_2$CHOH)$_2$] (**12**)[10] are all three-spin center homometallic ferromagnetic system while **3** shows weak antiferromagnetic interactions. This difference arises from the different carboxylate and μ_2-O bridges between Mn ions. In **2**, the ferromagnetic interactions between the Mn^{II} ions would be expected for the competitive effect of μ_2-O (Mn1–O4B–Mn2 angle = 108.7°) exchange pathway and one *syn–anti* carboxylate exchange pathway. In **3**, the antiferromagnetic interactions between the Mn^{II} ions would be anticipated because of both the effects of μ_2-O (Mn1–O5–Mn2 angle = 107.1°) exchange pathway and two *syn–syn* carboxylate exchange pathways. Compound **12** shows a three-spin center ferrimagnetic chain with a $-J_1J_1J_2-$ sequence, where the magnetic exchanges through the *syn–syn* carboxylate/μ_2-O bridge and the double *syn–anti* bridge are AF and F, respectively. In **4**, the antiferromagnetic interactions between the Mn^{II} ions are also expected in the [Mn$_4$(μ_2-COO)$_8$(μ_2-H$_2$O)] unit, due to the competitive effect of the μ_2-O (Mn2–O9–Mn2F angle = 110.4°, F = $-x+1, y, -z+{}^3/_2$) exchange pathway and other carboxylate exchange pathways. Though **5** and [Mn$_4$(tbip)$_4$(CH$_3$OH)$_2$]·2H$_2$O (**13**)[10] both have similar polymeric chains,

dx.doi.org/10.1021/ic3012537 | Inorg. Chem. 2012, 51, 9431–9442

5 shows weak antiferromagnetic interactions while **13** is an even-spin center homometallic ferromagnetic compound. In **5**, the antiferromagnetic interactions are found between Mn1 and Mn2 (or Mn1 and Mn3), relying on the effect of μ_2-O (Mn1−O8B−Mn2/Mn1−O5−Mn3 = 100.8/91.8°) exchange pathway and two *syn*−*syn* carboxylate exchange pathways. Compound **13** is a rare even-spin center homometallic ferrimagnetic compound, in which the ferrimagnetism arises from the nature of carboxylate bridging modes. It is also the first example of a 3D homometallic ferrimagnetic compound, featuring a ferrimagnetic helical chain with a (5/2, 15/2) spin topology and a $^1/_2$ magnetization plateau.

CONCLUSIONS

In summary, five Mn(II) coordination polymers with different polynuclear and polymeric chain units have been prepared under hydrothermal conditions, by using Mn^{II} and 5-*tert*-butyl isophthalic acid with the introduction of rationally selected flexible N-donor ancillary ligands. These complexes show 3D frameworks with different topologies. In **1**, the dimeric $[Mn_2O_2]$ units are interlinked into a 3D 6-connected polycatenane network with a new $(3^6.6^6.7^3)$ topology. The trimetallic $[Mn_3(COO)_6]$ units in **2** are extended to form a 3D 8-connected net with a $(3^6.4^{18}.5^3.6)$ topology. In **3**, the linear trimetallic $[Mn_3(COO)_6]$ units are linked by tbip to form an infinite chain, and the chains are further interlinked into a 3D pcu net by bib. In **4**, the tetranuclear $[Mn_4(\mu_2\text{-}COO)_8(\mu_2\text{-}H_2O)]$ units are linked by the organic backbones to generate a 3D 8-connected net with a $(3^6.4^{16}.5^6)$ topology. In **5**, the Mn^{II} chains in which $(\mu$-O$)(\mu$-COO) bridges alternate in an AABB sequence are extended into a 3D network with a $(4^3.6^2.8)_2(4^6.5^3.7)_2(4^9.5^2.6^4)_2(4^9.5^3.6^2.7)(4^9.6^5.8)$ topology. The overall structures of the coordination polymers mainly depend on the N-donor coligands used. Magnetic studies on **1**, **3**−**5** reveal that the above-mentioned mixed-bridging motifs show weak antiferromagnetic exchanges between the Mn^{II} ions while that in **2** induces weak ferromagnetic interactions therein.

ASSOCIATED CONTENT

Supporting Information

X-ray crystallographic information for **1**−**5** in CIF format, supplementary structural graphics for **2** and **4**, TGA plots and PXRD patterns for **1**−**5**, and temperature dependence of field-cooling (FC) χ_M for **1** and **4**. This material is available free of charge via the Internet at http://pubs.acs.org.

AUTHOR INFORMATION

Corresponding Author

*E-mail: wlya@lynu.edu.cn (L.-Y.W.), dumiao@public.tpt.tj.cn (M.D.).

Notes

The authors declare no competing financial interest.

ACKNOWLEDGMENTS

This work was supported by the National Natural Science Foundation of China (21073082 and 21071074), Program for New Century Excellent Talents in University (NCET-11-0947), and Program for Science & Technology Innovation Talents in Universities of Henan Province (No. 2011HASTIT027). M.D. also acknowledges the support from Tianjin Normal University.

REFERENCES

(1) (a) Yaghi, O. M.; Eddaoudi, M.; Kim, J.; Rosi, N.; Vodak, D.; Wachter, J.; O'Keeffe, M. *Science* **2002**, *295*, 469. (b) Chui, S. S.-Y.; Lo, S. M.-F.; Charmant, J. P. H.; Orpen, A. G.; Williams, I. D. *Science* **1999**, *283*, 1148. (c) Loiseau, T.; Volkringer, C.; Popov, D.; Guillou, N.; Férey, G.; Haouas, M.; Taulelle, F.; Mellot-Draznieks, C.; Burghammer, M.; Riekel, C. *Nat. Mater.* **2007**, *6*, 760. (d) Ni, Z.; Yassar, A.; Antoun, T.; Yaghi, O. M. *J. Am. Chem. Soc.* **2005**, *127*, 12752. (e) Férey, G. *Chem. Soc. Rev.* **2008**, *37*, 191. (f) Akine, S.; Taniguchhi, T.; Saiki, T.; Nabeshia, T. *J. Am. Chem. Soc.* **2005**, *127*, 540. (g) Yuan, D.; Zhao, D.; Sun, D.; Zhou, H.-C. *Angew. Chem., Int. Ed.* **2010**, *49*, 5357. (h) Schubert, U. *Chem. Soc. Rev.* **2011**, *40*, 575.

(2) (a) Sun, D.; Ma, S.; Ke, Y.; Collins, D. J.; Zhou, H.-C. *J. Am. Chem. Soc.* **2006**, *128*, 3896. (b) Nellutla, S.; Tol, J. V.; Dalal, N. S.; Bi, L. H.; Kortz, U.; Keita, B.; Nadjo, L.; Khitrov, G. A.; Marshall, A. G. *Inorg. Chem.* **2005**, *44*, 9795. (c) Tong, J. P.; Sun, X. J.; Tao, J.; Huang, R. B.; Zheng, L. S. *Inorg. Chem.* **2010**, *49*, 1289. (d) Boudalis, A. K.; Sanakis, Y.; Dahan, F.; Hendrich, M.; Tuchagues, J. P. *Inorg. Chem.* **2006**, *45*, 443. (e) Psycharis, V.; Raptopoulou, C. P.; Boudalis, A. K.; Sanakis, Y.; Fardis, M.; Diamantopoulos, G.; Papavassiliou, G. *Eur. J. Inorg. Chem.* **2006**, 3710. (f) Jiang, J. C.; Chu, Z. L.; Huang, W.; Wang, G.; You, X. Z. *Inorg. Chem.* **2010**, *49*, 5897. (g) Wu, S.-P.; Cowan, J. A. *Chem. Commun.* **2007**, 82. (h) Jeong, S.; Song, X.; Jeong, S.; Oh, M.; Liu, X.; Kim, D.; Moon, D.; Lah, M. S. *Inorg. Chem.* **2011**, *50*, 12133.

(3) (a) Papaefstathiou, G. S.; Perlepes, S. P. *Comments Inorg. Chem.* **2002**, *23*, 249. (b) Dendrinou-Samara, C.; Alexiou, M.; Zaleski, C. M.; Kampf, J. W.; Kirk, M. L.; Kessissoglou, D. P.; Pecoraro, V. L. *Angew. Chem., Int. Ed.* **2003**, *42*, 3763. (c) Winpenny, R. E. P. *Comments Inorg. Chem.* **1999**, *20*, 233. (d) Burger, J.; Klufers, P. *Angew. Chem., Int. Ed. Engl.* **1997**, *36*, 776. (h) Murray, K. S. *Adv. Inorg. Chem.* **1995**, *43*, 261. (e) Escuer, A.; Font-Bardia, M.; Kumar, S. B.; Solans, X.; Vicente, R. *Polyhedron* **1999**, *18*, 909. (f) Papaefstathiou, G. S.; Raptopoulou, C. P.; Tsohos, A.; Terzis, A.; Bakalbassis, E. G.; Perlepes, S. P. *Inorg. Chem.* **2000**, *39*, 4658. (g) Li, D. S.; Zhang, P.; Zhao, J.; Fang, Z. F.; Du, M.; Zou, K.; Mu, Y.-Q. *Cryst. Growth Des.* **2012**, *12*, 1697.

(4) (a) Boudalis, A. K.; Donnadieu, B.; Nastopoulos, V.; Clemente-Juan, J. M.; Mari, A.; Sanakis, Y.; Tuchagues, J. P.; Perlepes, S. P. *Angew. Chem., Int. Ed.* **2004**, *43*, 2266. (b) Libby, E.; Folting, K.; Huffman, C. J.; Huffman, J. C.; Christou, G. *Inorg. Chem.* **1993**, *32*, 2549. (c) Watton, S. P.; Fuhrmann, P.; Pence, L. E.; Caneschi, A.; Cornia, A.; Abbati, G.-L.; Lippard, S. J. *Angew. Chem., Int. Ed. Engl.* **1997**, *36*, 2774. (d) Nobumasa, K.; Takayuki, I.; Takashi, N.; Tamizo, K. *Polyhedron* **2008**, *27*, 2341. (e) Ribas, J.; Escuer, A.; Monfort, M.; Vicente, R.; Cortés, R.; Lezama, L.; Rojo, T. *Coord. Chem. Rev.* **1999**, *195*, 1027. (f) Winpenny, R. E. P. *Compr. Coord. Chem. II* **2004**, *7*, 125. (g) Jones, L. F.; Jensen, P.; Moubaraki, B.; Cashion, J. D.; Berry, K. J.; Murray, K. S. *Dalton Trans.* **2005**, 3344. (h) Ye, H. Y.; Zhang, L. Y.; Chen, J. L.; Chen, Z. N. *Chem. Commun.* **2006**, 1971.

(5) (a) Gui, L. C.; Wang, X. J.; Ni, Q. L.; Wang, M.; Liang, F. P.; Zou, H. H. *J. Am. Chem. Soc.* **2012**, *134*, 852. (b) Zheng, S. T.; Wu, T.; Chou, C.; Fuhr, A.; Feng, P.; Bu, X. *J. Am. Chem. Soc.* **2012**, *134*, 4517. (c) Park, K.; Pak, Y.; Kim, Y. *J. Am. Chem. Soc.* **2012**, *134*, 3524. (d) Roberts, J. M.; Fini, B. M.; Sarjeant, A. A.; Farha, O. K.; Hupp, J. T.; Scheidt, K. A. *J. Am. Chem. Soc.* **2012**, *134*, 3334. (e) Lu, W.; Yuan, D.; Makal, T. A.; Li, J.-R.; Zhou, H.-C. *Angew. Chem., Int. Ed.* **2012**, *51*, 1580. (f) Li, B.; Zhang, Z.; Li, Y.; Yao, K.; Zhu, Y.; Deng, Z.; Yang, F.; Zhou, X.; Li, G.; Wu, H.; Nijem, N.; Chabal, Y. J.; Lai, Z.; Han, Y.; Shi, Z.; Feng, S.; Li, J. *Angew. Chem., Int. Ed.* **2012**, *51*, 1412. (g) Stock, N.; Biswas, S. *Chem. Rev.* **2012**, *112*, 933.

(6) (a) Hoskins, B. F.; Robson, R. *J. Am. Chem. Soc.* **1990**, *112*, 1546. (b) Fondo, M.; Ocampo, N.; García-Deibe, A. M.; Sanmartín, J. *Eur. J. Inorg. Chem.* **2010**, 2376. (c) Gable, R. W.; Hoskins, B. F.; Robson, R. *J. Chem. Soc., Chem. Commun.* **1990**, 1677. (d) Liu, J. Q.; Liu, B.; Wang, Y. Y.; Liu, P.; Yang, G. P.; Liu, R. T.; Shi, Q. Z.; Batten, S. R. *Inorg. Chem.* **2010**, *49*, 10422. (e) Chen, Z.; Jia, M..; Zhang, Z.; Liang, F. *Cryst. Growth Des.* **2010**, *10*, 4806. (f) Zeng, M. H.; Zhou, Y. L.; Wu, M. C.; Sun, H. L.; Du, M. *Inorg. Chem.* **2010**, *49*, 6436. (g) Niu, C. Y.; Zheng, X. F.; Wan, X. S.; Kou, C. H. *Cryst. Growth Des.* **2011**, *11*, 2874.

(7) (a) Powell, A. K.; Heath, S. L.; Gatteschi, D.; Pardi, L.; Sessoli, R.; Spina, R.; Giallo, F. D.; Pieralli, F. *J. Am. Chem. Soc.* **1995**, *117*, 2491. (b) Rentschler, E.; Gatteschi, D.; Cornia, A.; Fabretti, A. C.; Barra, A. L.; Shchegolikhina, O. I.; Zhdanov, A. A. *Inorg. Chem.* **1996**, *35*, 4427. (c) Lippard, S. J. *Angew. Chem., Int. Ed. Engl.* **1988**, *27*, 344. (d) Caneschi, A.; Cornia, A.; Fabretti, A. C.; Gatteschi, D. *Angew. Chem., Int. Ed. Engl.* **1995**, *34*, 2862. (e) Li, D. S.; Fu, F.; Zhao, J.; Wu, Y. P.; Du, M.; Zou, K.; Dong, W. W.; Wang, Y. Y. *Dalton Trans.* **2010**, *39*, 11522. (f) Wei, Y.; Yu, Y.; Sa, R.; Li, Q.; Wu, K. *CrystEngComm* **2009**, *11*, 1054. (g) Chen, Q.; Zeng, M. H.; Wei, L. Q.; Kurmoo, M. *Chem. Mater.* **2010**, *22*, 4328. (h) Ling, Y.; Chen, Z.; Zheng, H.; Zhou, Y.; Weng, L.; Zhao, D. *Cryst. Growth Des.* **2011**, *11*, 2811.

(8) (a) Ma, S.; Sun, D.; Yuan, D.; Wang, X.-S.; Zhou, H.-C. *J. Am. Chem. Soc.* **2009**, *131*, 6445. (b) Ling, Y.; Yang, F.; Deng, M.; Chen, Z.; Liu, X.; Weng, L.; Zhou, Y. *Dalton Trans.* **2012**, *41*, 4007. (c) Zang, S. Q.; Dong, M.-M.; Fan, Y. J.; Hou, H.-W.; Mak, T. C. W. *Cryst. Growth Des.* **2012**, *12*, 1239. (d) Sarma, D.; Srivastava, V.; Natarajan, S. *Dalton Trans.* **2012**, *41*, 4135. (e) Ma, L. F.; Zhao, J. W.; Han, M. L.; Wang, L. Y.; Du, M. *Dalton Trans.* **2012**, *41*, 2078. (f) Eubank, J. F.; Wojtas, L.; Hight, M. R.; Bousquet, T.; Kravtsov, V. C.; Eddaoudi, M. *J. Am. Chem. Soc.* **2011**, *132*, 17532. (g) Chen, L. J.; Su, J. B.; Huang, R. B.; Lin, S.; Yang, M. X.; Huang, H. *Dalton Trans.* **2011**, *40*, 9731.

(9) Ma, S.; Sun, D.; Wang, X.-S.; Zhou, H.-C. *Angew. Chem., Int. Ed.* **2007**, *46*, 2458.

(10) Tian, C. B.; He, Z. Z.; Li, Z. H.; Lin, P.; Du, S. W. *CrystEngComm* **2011**, *13*, 3080.

(11) (a) Konar, S.; Mukherjee, P. S.; Drew, M. G. B.; Ribas, J.; Chaudhuri, N. R. *Inorg. Chem.* **2003**, *42*, 2545. (b) Waldo, G. S.; Yu, S.; Penner-Hahn, J. E. *J. Am. Chem. Soc.* **1992**, *114*, 5869. (c) Tan, X. S.; Xiang, D. F.; Tang, W. X.; Sun, J. *Polyhedron* **1997**, *16*, 689. (d) Policar, C.; Lambert, F.; Cesario, M.; Morgenstern-Badarau, I. *Eur. J. Inorg. Chem.* **1999**, 2201. (e) Delgado, F. S.; Kerbellec, N.; Ruiz-Perez, C.; Cano, J.; Lloret, F.; Julve, M. *Inorg. Chem.* **2006**, *45*, 1012.

(12) (a) Meng, M.; Zhong, D.-C.; Lu, T. B. *CrystEngComm* **2011**, *13*, 6794. (b) Zhang, X. M.; Wang, Y. Q.; Song, Y.; Gao, E. Q. *Inorg. Chem.* **2011**, *50*, 7284. (c) Lampropoulos, C.; Redler, G.; Data, S.; Abboud, K. A.; Hill, S.; Christou, G. *Inorg. Chem.* **2010**, *49*, 1325. (d) Berggren, G.; Huang, P.; Eriksson, L.; Styring, S.; Anderlund, M. F.; Thapper, A. *Dalton Trans.* **2010**, *39*, 11035. (e) Li, Y.; Zou, W. Q.; Wu, M. F.; Lin, J. D.; Zheng, F. K.; Liu, Z. F.; Wang, S. H.; Guo, G. C.; Huang, J. S. *CrystEngComm* **2011**, *13*, 3868.

(13) (a) Wang, Y. Q.; Sun, Q.; Yue, Q.; Cheng, A. L.; Song, Y.; Gao, E. Q. *Dalton Trans.* **2011**, *40*, 10966. (b) Wang, X. F.; Zhang, Y. B.; Zhang, W. X.; Xue, W.; Zhou, H. L.; Chen, X. M. *CrystEngComm* **2011**, *13*, 4196. (c) Ma, C. B.; Hu, M. Q.; Chen, H.; Wang, M.; Zhang, C. X.; Chen, C. N.; Liu, Q. T. *CrystEngComm* **2010**, *12*, 1467. (d) Chen, W. X.; Zhuang, G. L.; Zhao, H. X.; Long, L. S.; Huang, R. B.; Zheng, L. S *Dalton Trans.* **2011**, *40*, 10237. (e) Ren, Y. X.; Xiao, S. S.; Zheng, X. J.; Li, L. C.; Jin, L. P. *Dalton Trans.* **2012**, *41*, 2639.

(14) (a) Ma, L. F.; Wang, L. Y.; Wang, Y. Y.; Du, M.; Wang, J. G. *CrystEngComm* **2009**, *11*, 109. (b) Ma, L. F.; Wang, L. Y.; Du, M. *CrystEngComm.* **2009**, *11*, 2593. (c) Han, M. L.; Li, S. H.; Ma, L. F.; Wang, L. Y. *Inorg. Chem. Commun.* **2012**, *20*, 340.

(15) Sheldrick, G. M. *Acta Crystallogr.* **2008**, *A64*, 112.

(16) Jin, R. F.; Yang, S. Y.; Li, H. M.; Long, L. S.; Huang, R. B.; Zheng, L. S. *CrystEngComm* **2012**, *14*, 1301.

(17) Zhou, D. S.; Wang, F. K.; Yang, S. Y.; Xie, Z. X.; Huang, R. B. *CrystEngComm* **2009**, *11*, 2548.

(18) Ma, L. F.; Wang, L. Y.; Lu, D. H.; Batten, S. R.; Wang, J. G. *Cryst. Growth Des.* **2009**, *9*, 1741.

(19) Carlin, R. L. *Magnetochemistry*; Springer: Berlin, 1986.

(20) Kahn, O. *Molecular Magnetism*; VCH Publisher: New York, 1993.

(21) Curély, J. *Europhys. Lett.* **1995**, *32*, 529. (b) Curély, J. *Physica B* **1998**, *245*, 263. (c) Curély, J. *Physica B* **1998**, *254*, 277. (d) Curély, J.; Rouch, J. *Physica B* **1998**, *254*, 298.

(22) Sun, Q.; Cheng, A. L.; Wang, Y. Q.; Ma, Y.; Gao, E. Q. *Inorg. Chem.* **2011**, *50*, 8144.

(23) Zhao, J. P.; Hu, B. W.; Yang, Q.; Zhang, X. F.; Hu, T. L.; Bu, X. H. *Dalton Trans.* **2010**, *39*, 56.

(24) (a) Wang, Y. Q.; Jia, Q. X.; Wang, K.; Cheng, A. L.; Gao, E. Q. *Inorg. Chem.* **2010**, *49*, 1551. (b) Zhang, X. M.; Wang, Y. Q.; Li, X. B.; Gao, E. Q. *Dalton Trans.* **2012**, *41*, 2026.

(25) Fisher, M. E. *Am. J. Phys.* **1964**, *32*, 343.

(26) (a) Abu-Youssef, M. A. M.; Escuer, A.; Goher, M. A. S.; Mounter, F. A.; Reib, G. J.; Vicente, R. *Angew. Chem., Int. Ed.* **2000**, *39*, 1624. (b) Cano, J.; Journaux, Y.; Goher, M. A. S.; Abu-Youssef, M. A. M.; Mautner, F. A.; Reib, G. J.; Escuer, A.; Vicente, R. *New J. Chem.* **2005**, *29*, 306. (c) Abu-Youssef, M. A. M.; Drillon, M.; Escuer, A.; Goher, M. A. S.; Mautner, F. A.; Vicente, R. *Inorg. Chem.* **2000**, *39*, 5022.

(27) (a) Goodenough, J. B. *Magnetism and the Chemical Bond*; Wiley: New York, 1963. (b) Wang, Z. M.; Zhang, B.; Fujiwara, H.; Kobayashi, H.; Kurmooc, M. *Chem. Commun.* **2004**, 416. (c) Tang, Y. Z.; Wang, X. S.; Zhou, T.; Xiong, R. G. *Cryst. Growth Des.* **2006**, *6*, 11.

(28) (a) Rodríguez-Fortea, A.; Alemany, P.; Alvarez, S.; Ruiz, E. *Chem.—Eur. J.* **2001**, *7*, 627. (b) Maji, T. K.; Sain, S.; Mostafa, G.; Lu, T. H.; Ribas, J.; Monfort, M.; Chaudhuri, N. R. *Inorg. Chem.* **2003**, *42*, 709.

(29) Gómez, V.; Corbella, M.; Font-Bardia, M.; Calvet, T. *Dalton Trans.* **2010**, *39*, 11664.

(30) (a) Yamase, T.; Ishikawa, H.; Abe, H.; Fukaya, K.; Nojiri, H.; Takeuchi, H. *Inorg. Chem.* **2012**, *51*, 4606. (b) Viciano-Chumillas, M.; Tanase, S.; Mutikainen, I.; Turpeinen, U.; de Jongh, L. J.; Reedijk, J. *Dalton Trans.* **2009**, 7445.

(31) (a) Miyasaka, H.; Nezu, T.; Iwahori, F.; Furukawa, S.; Sugimoto, K.; Clérac, R.; Sugiura, K.-i.; Yamashita, M. *Inorg. Chem.* **2003**, *42*, 4501. (b) Zhang, S.; Zhen, L.; Xu, B.; Inglis, R.; Li, K.; Chen, W.; Zhang, Y.; Konidaris, K. F.; Perlepes, S. P.; Brechin, E. K.; Li, Y. *Dalton Trans.* **2010**, *39*, 3563.

(32) (a) Chang, H.; Larsen, S. K.; Boyd, P. D. W.; Pierpont, C. G.; Hendrickson, D. N. *J. Am. Chem. Soc.* **1988**, *110*, 4565. (b) Wesolek, M.; Meyer, D.; Osborn, J. A.; Cian, A. D.; Fischer, J.; Derory, A.; Legoll, P.; Drillon, M. *Angew. Chem., Int. Ed. Engl.* **1994**, *33*, 1592.